Bull Volcanol (1992) 54:347–360

Bulletin of
Volcanology

Evolution of the Olympus Mons Caldera, Mars

Peter J Mouginis-Mark and Mark S Robinson

Planetary Geosciences, Department of Geology and Geophysics, School of Ocean and Earth Science and Technology, University of Hawaii, Honolulu, HI, 96822, USA

Received July 30, 1991/Accepted January 6, 1992

Abstract. Synoptic images of the Martian volcano Olympus Mons are of a quality and quantity that are unique for Mars and, somewhat surprisingly, are appreciably better than image data that exist for many volcanoes on Earth. Useful information about the evolution of shield volcanoes on Earth can thus be derived from the investigation of this extraterrestrial example. We have used shadow-length measurements and photoclinometrically derived profiles to supplement and refine the topographic map of the Olympus Mons caldera. As much as 2.5 km of collapse took place within the 80×65 km diameter caldera and the elevation of the caldera rim varies by almost 2.0 km (low around the oldest collapse events, high around the youngest). An eight-stage evolutionary sequence for the caldera of Olympus Mons is identified which shows that caldera subsidence was a longterm process rather than the near-instantaneous event that has been interpreted from comparable terrestrial examples. Tectonic features on the caldera floor indicate a transition from an extensional environment (graben formation) around the perimeter of the caldera to compression (ridge formation) towards the caldera center. This transition from a compressional to extensional environment is surprisingly sudden, occurs at a radial distance of ~ 17 km from the caldera center, and is import because it can be used to infer that the magma chamber was relatively shallow (thought to be at a depth of $< \sim 16$ km beneath the caldera floor; Zuber and Mouginis-Mark 1990). Ample evidence is also found within the Olympus Mons caldera for solidified lava lakes more than 30 km in width, and for the localized overturning and/or withdrawal of lava within these lakes.

Introduction

Olympus Mons on Mars (Fig. 1) is one of the largest volcanoes in the Solar System, and is frequently compared to Mauna Loa in Hawaii in terms of its morphology and probable style of eruption (cf. Carr and Greeley 1980). Olympus Mons is located at 18°N, 133°W in the Tharsis region of Mars. The volcano has a basal diameter in excess of 600 km, rises more than 25 km above the surrounding plains, and has a basal escarpment that in places exceeds 6 km in height (Wu et al. 1984). The summit caldera of Olympus Mons exhibits excellent examples of tectonic processes associated with shield volcanism on Mars (Mouginis-Mark et al. 1991). Within the 80×65 km diameter structure are six nested craters (Fig. 2) that indicate that the volcanic edifice has undergone multiple collapse episodes. Also found within the caldera are numerous tectonic features that have been interpreted to be formed by compression (wrinkle ridges) and extension (graben) (Greeley and Spudis 1981).

Extensive high-resolution (15–20 m/pixel) coverage of Olympus Mons from the Viking Orbiter 1 spacecraft permits the investigation of the sequence of subsidence and tectonic events associated with the evolution of the nested summit caldera, thereby extending previous studies of this complex caldera (Mouginis-Mark 1981). These data for the volcano permit a detailed morphological analysis to be carried in a setting where, unlike on Earth, erosion has not masked the underlying geologial process. The synoptic image data that are available for Olympus Mons are of a quality and quantity that are unique for Mars and, somewhat surprisingly, are appreciably better than image data that exist for many volcanoes on Earth.

Stereogrammetrically derived topographic data (obtained from a total of 103 Viking images) have been used to produce a 200 m-interval contour map of Olympus Mons (Wu et al. 1984). In addition, Viking Orbiter images with various lighting geometries also permit detailed analysis of the landforms on the caldera floor. The availability of the topographic map (Wu et al. 1984), shadow measurements, and photoclinometric techniques (Davis and Soderblom 1984) that permit quantitative measurement of the heights and slopes of features on the caldera floor, have enabled us to reassess

Correspondence to: P Mouginis-Mark

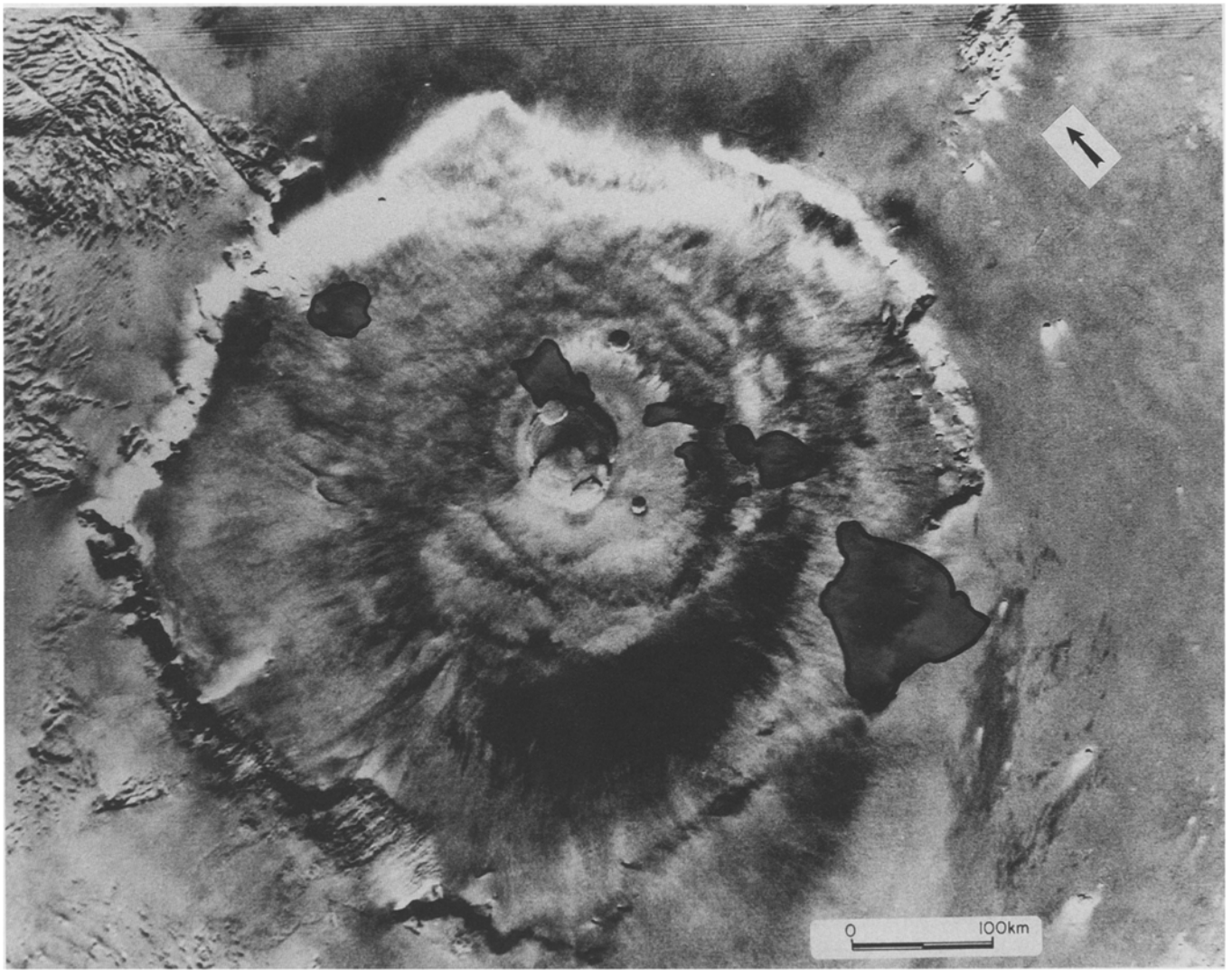

Fig. 1. Image of Olympus Mons with the major Hawaiian islands drawn for scale comparison. The summit of Olympus Mons rises more than 25 km above the surrounding plains, and the basal diameter is about 600 km. *Arrow* points north. Viking Orbiter frame 646A28

the geologic evolution of the Olympus Mons caldera as a first step towards the numerical modeling of the evolution of the magma chamber (Zuber and Mouginis-Mark 1990). Here we first describe the topographic character of the summit region of the volcano, identify the different types of tectonic features that are found within the caldera, and then use the distribution of these features to refine the chronology for the evolution of the summit. We conclude by making some inferences about the unique character of this Martian shield compared to analogs drawn from the Earth and Mars, and note possible instances where Olympus Mons might provide insights into the process of caldera collapse on Earth.

Caldera topography

We have inspected the high-resolution Viking Orbiter images obtained late in the Survey Mission and have found that in a few places the lower-resolution topographic map of Wu et al. (1984) does not conform to the interior morphology of the summit. We have therefore used shadow-length measurements and photoclinometrically derived profiles to supplement and refine the topographic map of the caldera (Fig. 3). Shadow-length measurements can be made for any area of Mars provided that the Sun is sufficiently low to cast a shadow, that the illumination geometry is known, and that the length of the shadow cast by an obstacle is numerous data points (pixels) in size (Robinson 1990); the Viking Orbiter data of Olympus Mons make such shadow measurements particularly easy due to the low Sun angle and high spatial resolution (Fig. 4). The photoclinometry technique that we have employed (the asymmetric method of Davis and Soderblom 1984) uses calibrated digital pixel values to calculate a slope and change in height across a pixel of known width. The advantages of the photoclinometry method is that it can be applied to single (monoscopic) images, permitting the digital data to be used to investigate the topography of areas where no

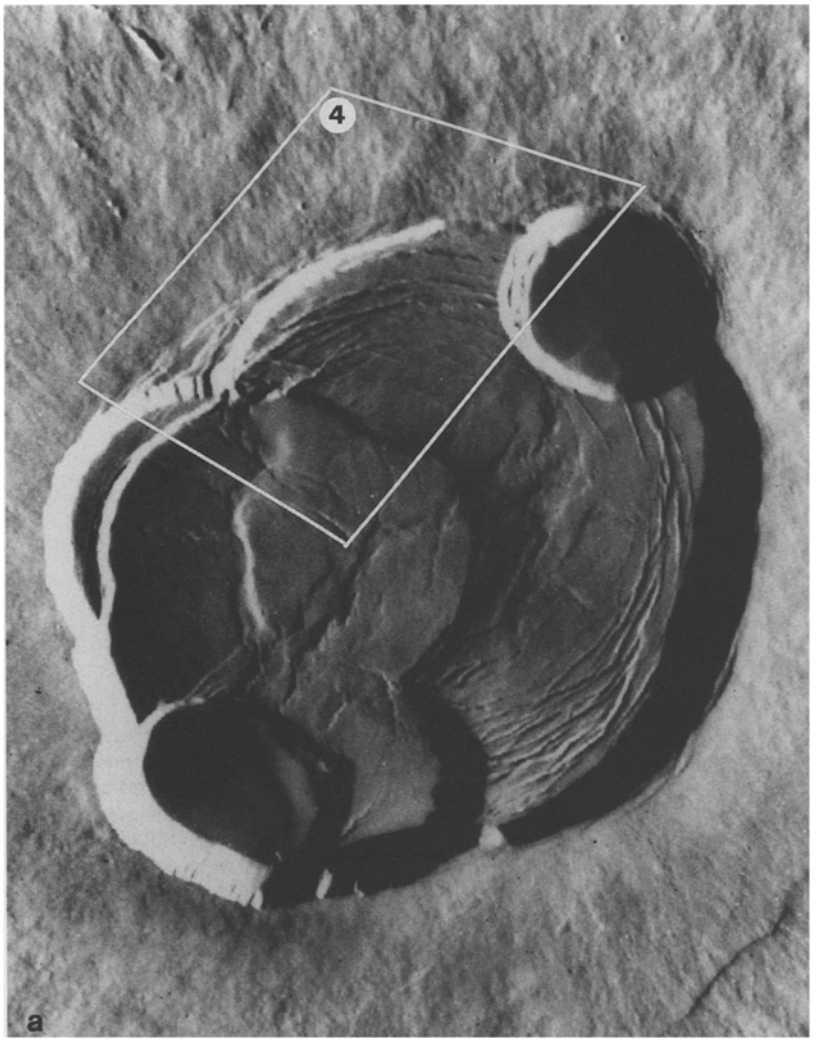

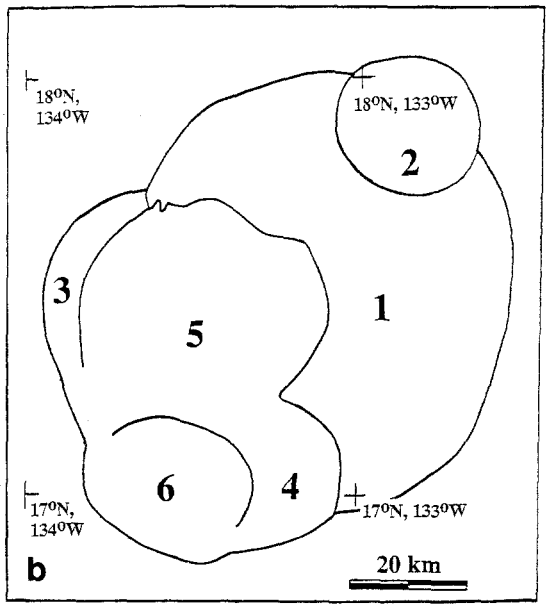

Fig. 2. a Viking Orbiter view of the summit caldera of Olympus Mons, showing the six nested craters and the prominent wrinkle ridges and graben. Illuminations is from the right, width of image equivalent to 80 km, and north is towards top of the image. *Outlined area* shows the approximate location of Fig. 4. Viking Orbiter frame number 890A68 (160 m/pixel). **b** Sketch map of the summit of Olympus Mons, showing the six nested craters (*1* through *6*) identified by Mouginis-Mark (1981). Based on superposition relationships (see text), crater 1 appears to be the oldest and 6 the youngest

stereo data exist. By selecting areas that are assumed to have constant albedo, topographic profiles across a landform can be derived from the pixel-by-pixel variation in brightness across the image due to changes in local slope. This method appears valid within the caldera because albedo variations should be minimal due to an inferred monochromatic cover of dust. A summation of the slopes determined by photoclinometry, when multiplied by the pixel resolution, permits a topographic profile to be determined.

Our method for generating this revised topographic map involved first assuming that the rim crest topography of the caldera was accurately determined by the stereographic measurements of Wu et al. (1984). This assumption is reasonable because the rim is an easily identified feature in stereo images. Using calibrated Viking Orbiter images with Sun incidence angles in excess of 70° (frames 890A68, 475S03 and 475S07), we determined the heights of the caldera walls from the digital data using shadow-length measurements and trigonometry. These wall heights were then used to set the reference surface for the perimeter of the caldera floor. Three photoclinometric profiles (see Fig. 3 for locations) were then derived with respect to this new floor perimeter reference surface in order to determine the interior slopes of the caldera. In deriving these profiles we assumed that the caldera surface had a uniform albedo and that the floor has no unusual sub-pixel scale photometric properties. The final step in the generation of our revised contour map involved contouring the new elevation measurements using the trends within the caldera identified by Wu et al. (1984), and our geomorphic interpretation of features within the caldera.

Analysis of the stereogrammetrically derived topography of Olympus Mons shows that the floor of the caldera is at an elevation of 22.9–24.6 km above the reference surface of Mars (the 6.1 mb atmospheric pressure level). Due to the illumination geometry (incidence angle = 70–80°) and pixel size (15–156 m), our shadow measurements have a height error of ±85 m for the eastern side of the caldera and ±15 m for the western side, assuming that the top and bottom of the shadow are located within 3 pixels in each image. These shadow measurements show that the walls are in excess of 600 m high around the entire caldera, and that the soutern rim exceeds 3.0 km in height. The floor of crater 1 (Fig. 3) has a maximum slope of ~5° down towards the center of the caldera, with a change in elevation in excess of

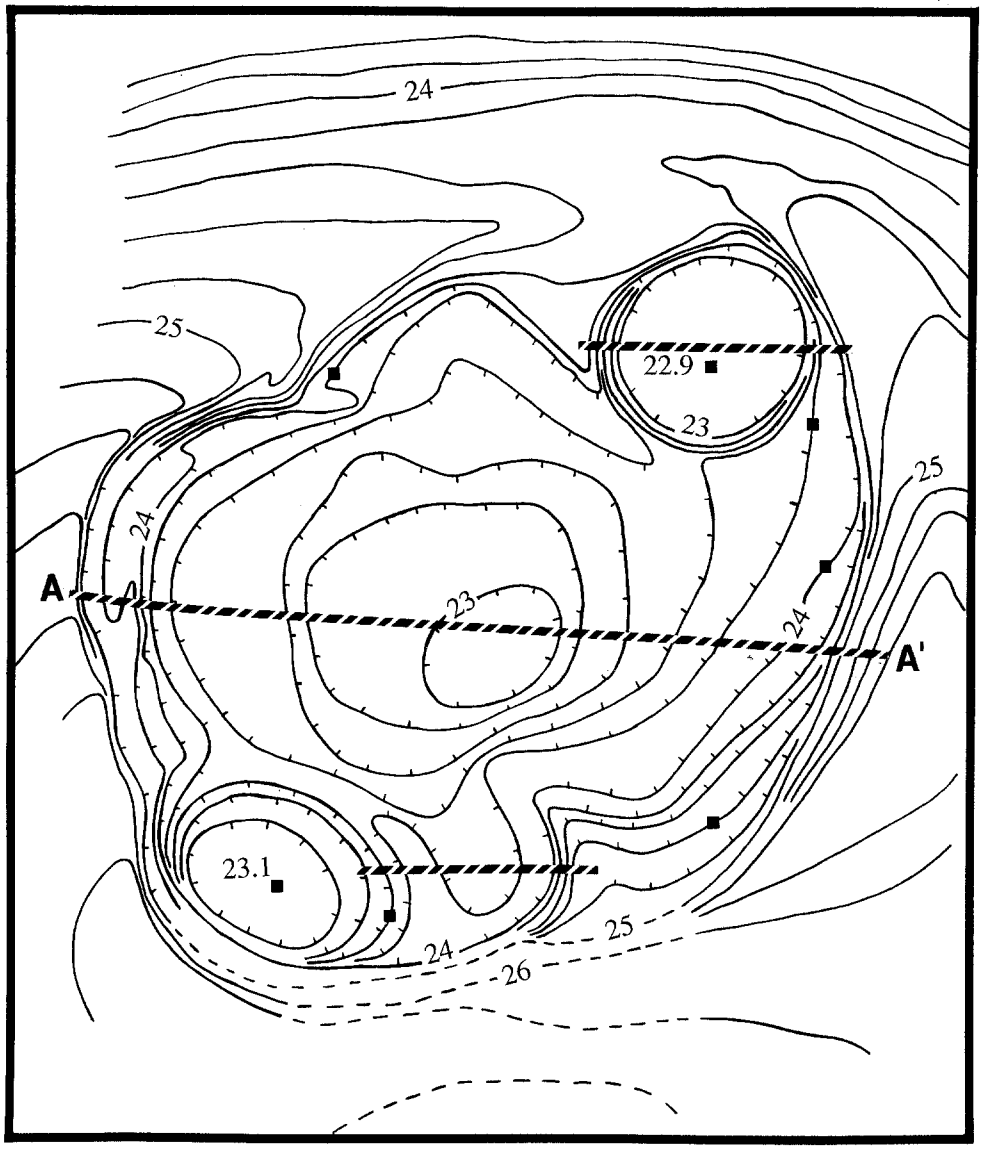

Fig. 3. Topographic map of the caldera of Olympus Mons derived by Wu et al. (1984) and modified in this analysis to include our shadow-length and photoclinometric measurements of slopes and scarp heights. Elevations are in kilometers above the 6.1 mb reference surface of Mars, contour interval is 200 m. *Dashed lines* show the locations of the profiles derived by photoclinometry. *Line A–A'* is the profile shown in Fig. 5a; *solid squares* are points where the rim height was derived by shadow-length measurements

1.2 km east of the caldera center (Fig. 5a). The rim of the caldera also shows considerable relief (Fig. 5b). The northern rim is at an elevation of ~24.4 km, while the southern rim of crater 6, inferred to be the youngest crater based on superposition relationships (Mouginis-Mark 1981), exceeds 26.2 km elevation. Possible causes of this variation of the rim elevation are discussed below.

Distribution of tectonic features

Mouginis-Mark et al. (1990) identified both compressional and extensional features on the floor of the Olympus Mons caldera. Compressional features include broad (1–3 km wide) ridges that are morphologically similar to wrinkle ridges on the Moon and narrower (<1 km width) linear ridges that are approximately circumferential to the perimeter of crater 1 (Fig. 6a). There has been considerable debate about the origin of the lunar and planetary wrinkle ridges, but the consensus opinion is that they are compressional in origin and are predominately formed in layered rocks that are typically volcanic in origin (cf. Plescia and Golombek 1986; Sharpton and Head 1988). A topographic profile across one of the larger wrinkle ridges (Fig. 5a) shows that it is >300 m high on its eastern side and 2 km wide. Typical planar dimensions for the wrinkle ridges on the floor of craters 1 and 5 are 0.8–1.4 km in width and 3.0–15.0 km in length. Maximum dimensions for the largest ridge are 1.8 km width and 23.0 km length.

An extensive series of graben around the perimeter of crater 1 is the primary extensional feature found within the caldera (Fig. 6b) although additional narrow fractures can be seen both on the caldera floor and rim (Fig. 6c). We are confident that these features are indeed graben because of their symmetrical geometry (two bounding faults), flat floors, and approximately constant width. The larger of these graben are ~420–450 m wide, may extend for more than 25 km in length, and shadow-length measurements (from frame 473S28) show that they are ~180–200 m deep. The smaller fractures

Fig. 4. Oblique view of the western side of the Olympus Mons summit caldera, showing the location of shadows (*arrowed*) on the caldera floor. Knowledge of the illumination geometry and the pixel resolution permit the height of the caldera wall to be calculated from data such as these. Note that image data from which the shadow measurements were derived have a spatial resolution of 28 m/pixel on the western side of the caldera, and data for the eastern side have a resolution of 160 m/pixel. See Fig. 2a for location. Viking Orbiter image 475S03 (INA = 80°)

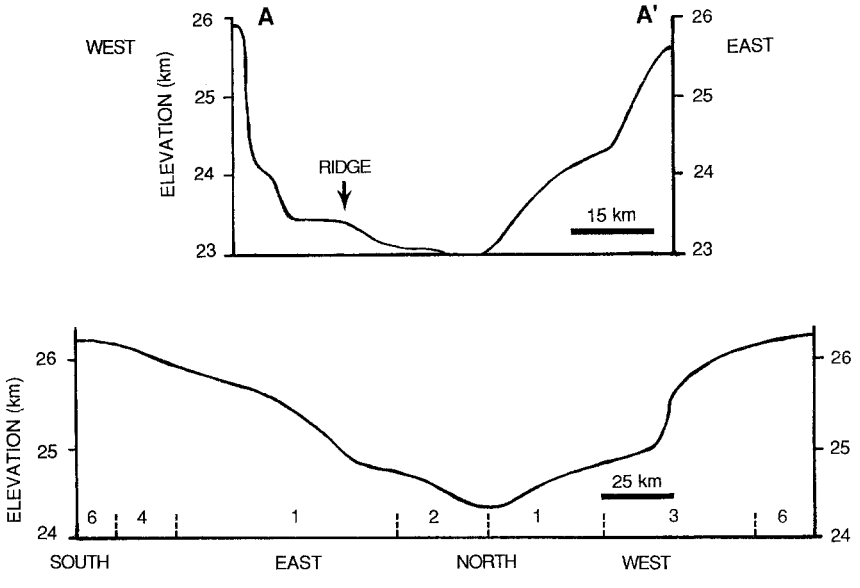

Fig. 5. a (Top): Photoclinometrically derived profile across the floor of Olympus Mons caldera, showing the variation in slope across the floors of craters 1, 3 and 5, and the location of the prominent wrinkle ridge on the floor of crater 5. Vertical exaggeration is 14.2×, data derived from Viking Orbiter image 890A68. See Fig. 3 for location. **b** (Bottom): Rim profile (i.e. the sharp edge between the summit flanks and the caldera wall – see Fig. 2a) around the Olympus Mons caldera. The variation in elevation is >2.0 km. Using the topographic map (Fig. 3), the elevation of the rim of crater 6 is seen to be 1.9 km higher than the rim of crater 2, and >1.5 km higher than much of crater 1. Vertical exaggeration is 31.5×. Compass directions indicated on horizontal axis, and boundaries between craters (*numbered*) are shown by *vertical dashed lines*

are typically 100 m in width, <5 km in length, and are too shallow to confidently determine their depths at an image resolution of ~15 m/pixel.

The highest spatial resolution Viking Orbiter images that exist for Olympus Mons (~12 m/pixel) allow the distribution and possible mode of formation of these tectonic features to be investigated in areas where such data are available. We interpret that the formation of both the circumferential graben and narrow circumferential ridges on the floor of crater 1 were formed prior

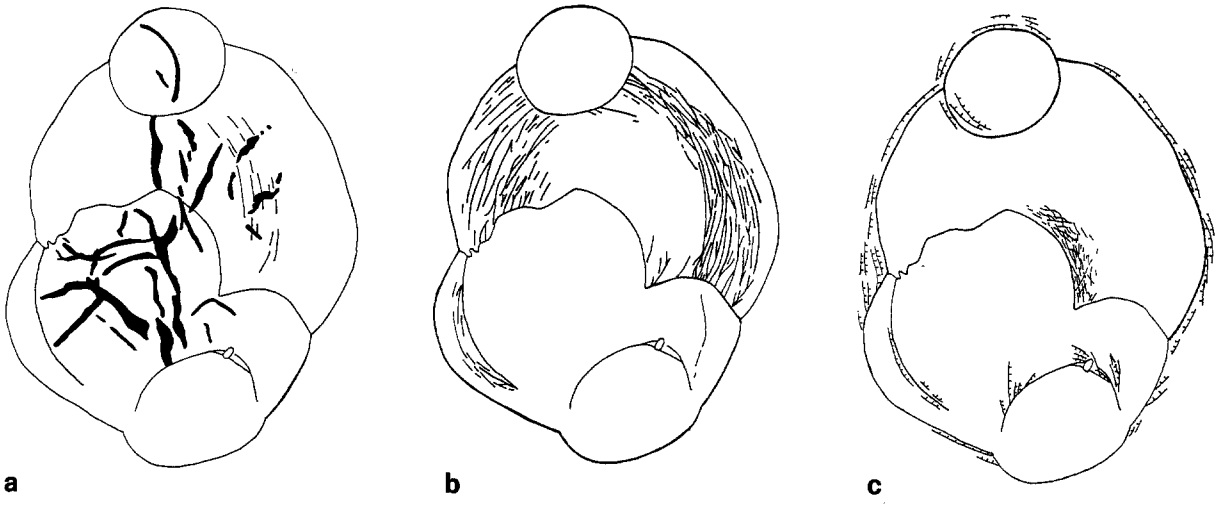

Fig. 6. **a** Distribution of wrinkle ridges and linear concentric ridges (narrow features) within the caldera of Olympus Mons. Mapped from a combination of Viking Orbiter images obtained on orbits 360A, 890A, 461S, 473S, 474S and 475S. **b** Distribution of large circumferential graben on the floor of Olympus Mons caldera. Mapped from the same data base as Fig. 6a. **c** Distribution of small linear fractures on the floor and rim of Olympus Mons caldera. *Barbed lines* denote step faults; *lines* are cracks on floor of crater 1. Mapped from the same data base as Fig. 6a

to flooding of craters 4 and 5, since the latest surface of craters 4 and 5 is relatively smooth and evidently cover any graben or ridges that may have been inherited from crater 1. Figures 7 and 8 show that the radial wrinkle ridges in crater 1 are cut by both the circumferential graben and the narrow circumferential ridges. It is evident that within crater 1 the central portion of the caldera floor was most recently in a state of compression during its evolution; following the resurfacing of the floor, the perimeter of the caldera floor was an extensional environment. In an east-west direction, the transition that is preserved from compression in the center of the caldera to extension around the perimeter is very rapid, and occurs at a radial distance of ~17 km from the center of the 33-km-radius caldera. The spatial distribution of the circumferential ridges and graben indicates that relatively protracted floor subsidence took place; after the initial collapse, the floor formed from a cooled lake than then subsided in its central region. This lack of catastrophic collapse of the central portion of the floor has significance for the distribution of stress that existed during the subsidence. Indeed, the distribution of the intra-caldera tectonic features has been used to infer a magma chamber depth for Olympus Mons at the time of caldera subsidence of less than ~16 km beneath the caldera floor (Zuber and Mouginis-Mark 1990).

Within craters 4 and 5 there are numerous narrow linear ridges (Fig. 9). These linear ridges are typically <100 m wide, <5 km in length, and have slopes that are so shallow (less than the solar incidence angle on the images; i.e. <~15°) that their heights cannot be measured from their shadow lengths (i.e. they are probably <~20 m high). Linear ridges appear to be superimposed upon the wrinkle ridges, and often traverse the crater floor, a wrinkle ridge, and back to the crater floor without changing their orientation (Fig. 10). The small size and their occurrrence upon the broader wrinkle ridges suggest to us that these linear ridges are older features than the wrinkle ridges, because otherwise their orientations and locations would have been constrained by the wrinkle ridges. We interpret the wrinkle ridges to be the products of compression during the subsidence of the entire caldera floor, and the linear ridges to be folds in the lava surface produced when the caldera floor was forming, analogous to pressure ridges that form on the surface of terrestrial lava lakes (cf. Peck and Kinoshita 1976). Several irregular collapse pits and sinuous troughs can also be found on the floor of crater 5, and these features may also have formed during the solidification of the surface of a lava lake by localized draining of the near-surface magma (we have observed comparable features on the surface of the September 1982 Kilauea lava flow, Hawaii, where drain-back down the vent followed the termination of activity, and left several irregular-shaped pits at the surface).

It is instructive to correlate the distribution of the geomorphic features on the caldera floor of Olympus Mons with the topographic data described in the previous section. A comparison of Figs. 3 and 6 shows that the circumferential graben and circumferential ridges parallel the contours of craters 1 and 3, and the circumferential ridges in crater 1 (Fig. 8) are located at a slight break in slope on the eastern part of the caldera floor. The linear ridges that are common on the floors of craters 4 and 5 (at elevations between 23.0–23.8 km) are absent from topographically higher parts of the caldera floor that exceed an elevation of 23.8 km. On the northwest and southeast rims, block faulting has taken place on walls that are <1.0 km high, while on the southern rim of crater 6 (over 3.0 km high) the wall rocks show no signs of incipient failure, suggesting that there are spatial variations in the mechanical strength of the wall rocks around the perimeter of the caldera.

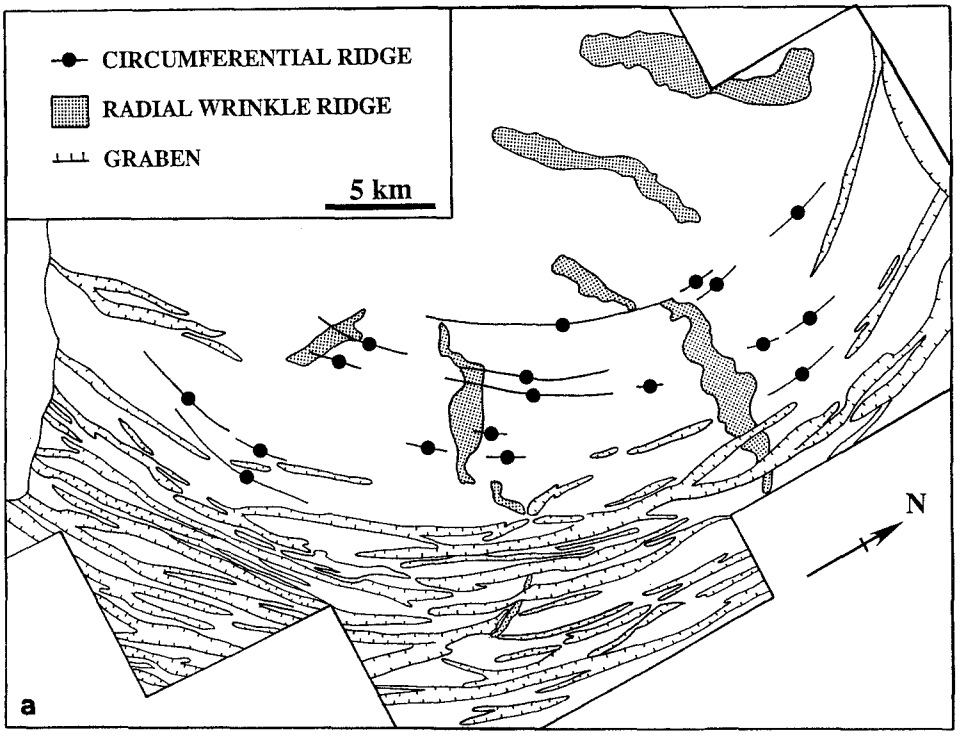

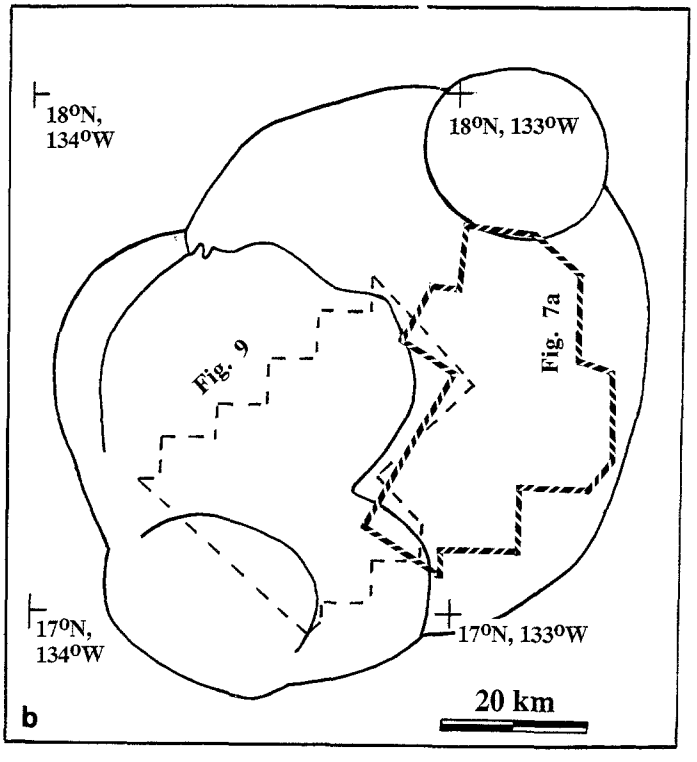

Fig. 7. a Distribution of circumferential graben and ridges, and radial wrinkle ridges within the oldest portion (crater 1) of the Olympus Mons caldera. Note that the graben are truncated by the wall to crater 4, and that the wrinkle ridges are cut by the graben. See Fig. 7b for location. Mapped from Viking Orbiter frames 473S27-29, 474S25-30. **b** Location map for areas shown in Figs. 7a and 9

Chronology of intra-caldera events

The sequence of intra-caldera deformation events is particularly well illustrated at Olympus Mons by image data collected on orbits 473S and 474S of Viking Orbiter 1 (Figs. 6 and 8). These images cover both the oldest and youngest portions of the caldera floor. Our observations permit the following eight-stage chronology for the caldera floor to be inferred:

Stage 1: The first preserved summit event was the catastrophic collapse and subsequent partial infilling of crater 1, which essentially defines the boundary of the caldera. Our shadow-length measurements of the preserved wall (from Viking frame 890A68, 156 m/pixel) indicate that at least 1100 ± 57 m of collapse was associated with this event. Talus from this collapse is interpreted to be now buried beneath younger materials.

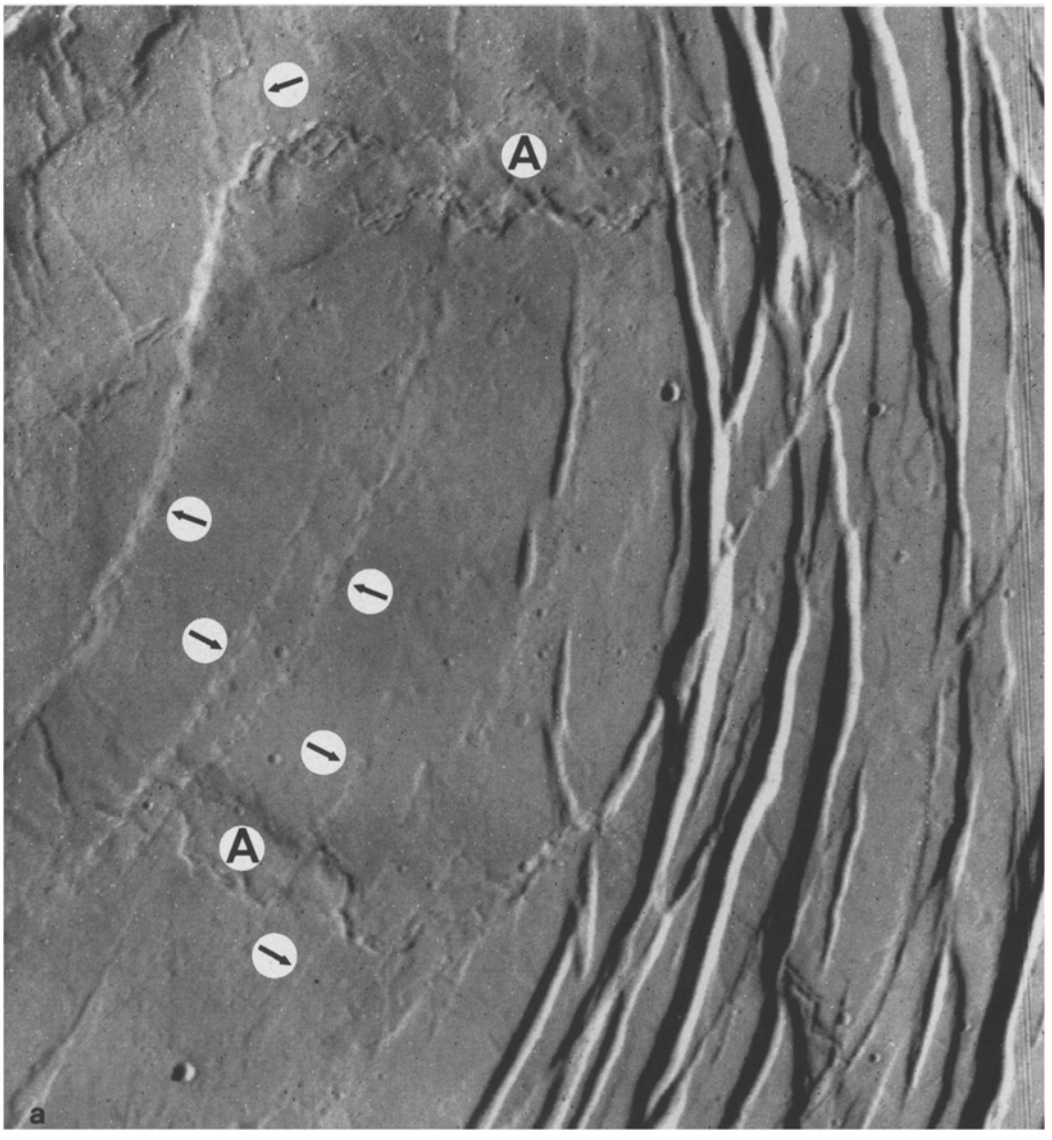

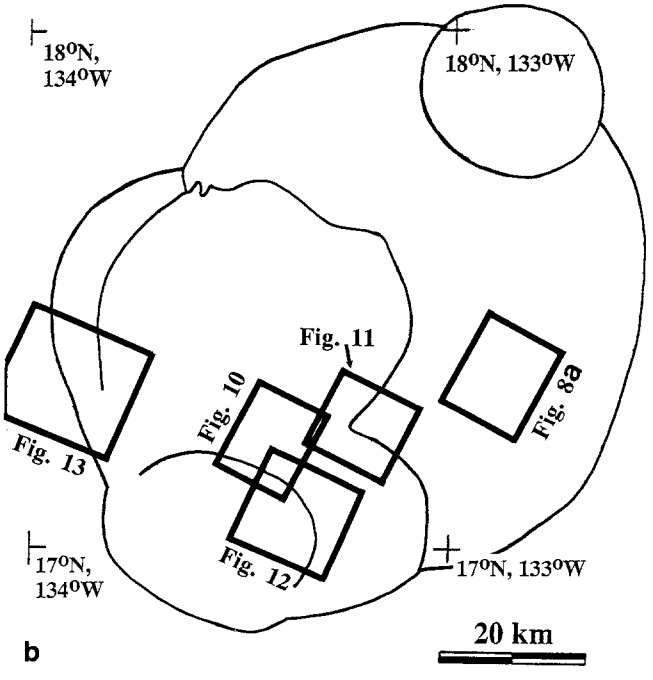

Fig. 8. a Viking Orbiter view of the transition zone between compression (left) and extension (right) within crater 1 at a radial distance of ~17 km from the caldera center. *A* identifies radial wrinkle ridges that are cut by the circumferential graben. *Arrows* show the narrow circumferential ridges. See Fig. 8b for location. Frame number 473S30 (14 m/pixel). Width of image equivalent to 15 km. **b** Location map for areas shown in Figs. 8a, 10, 11, 12 and 13

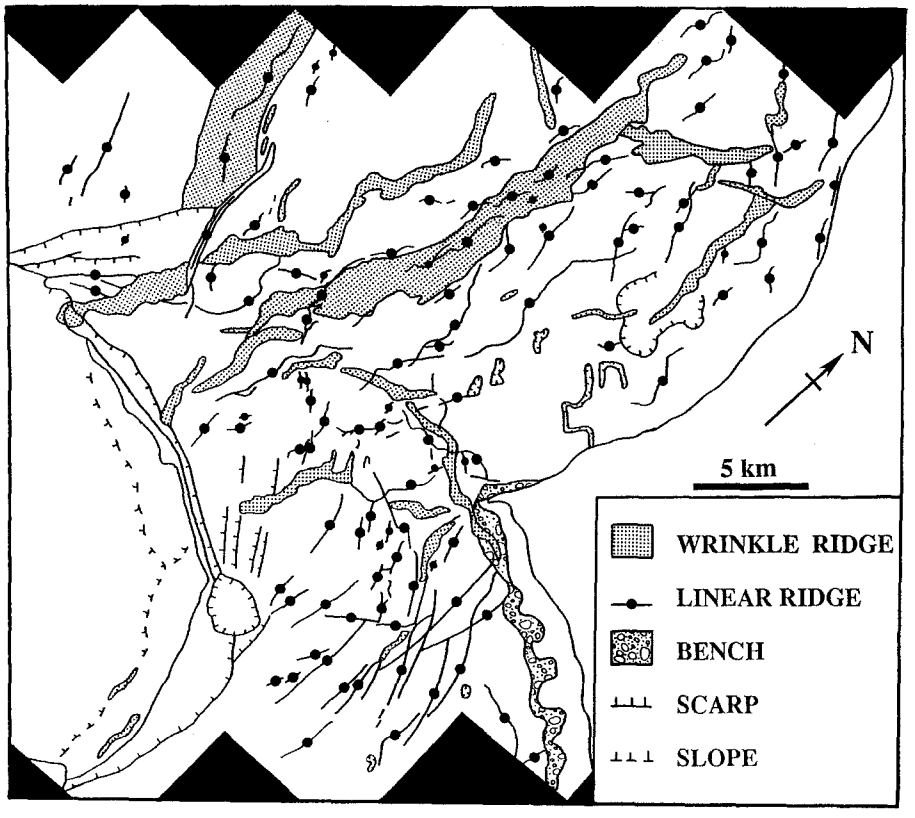

Fig. 9. Complex series of linear ridges on the floor of craters 4 and 5 indicate that a large overturning lava lake may have existed soon after the initial collapse event. Linear ridges are superposed upon the younger wrinkle ridges, and a bench exists around the perimeter of crater 4. See Fig. 7b for location. Mapped from Viking Orbiter frames 473S17-26

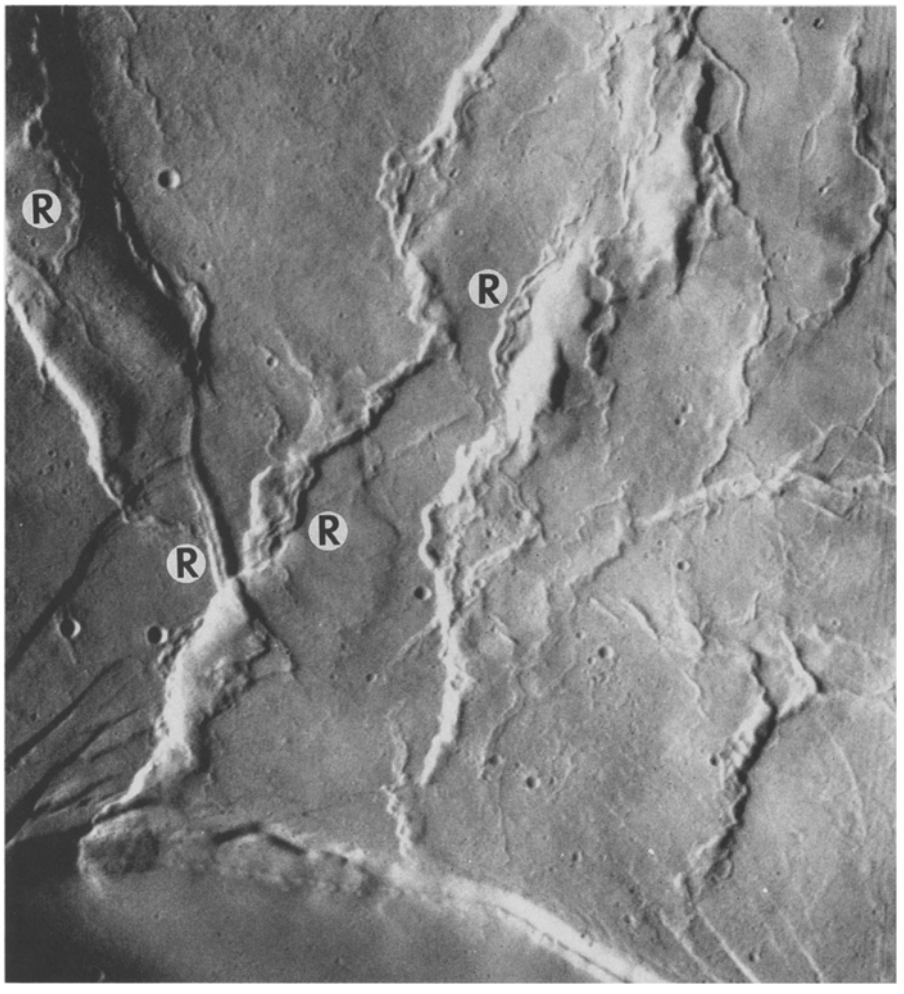

Fig. 10. Multiple linear ridges and wrinkle ridges are seen at the boundary between craters 4 and 5. Note the general N–S orientation to many of the linear ridges, and that some of them are paired ridges (e.g. at *R*) with a central depression. Illumination direction is from the left, image width is 18 km. See Fig. 8b for location. Viking Orbiter frame 473S21 (15 m/pixel)

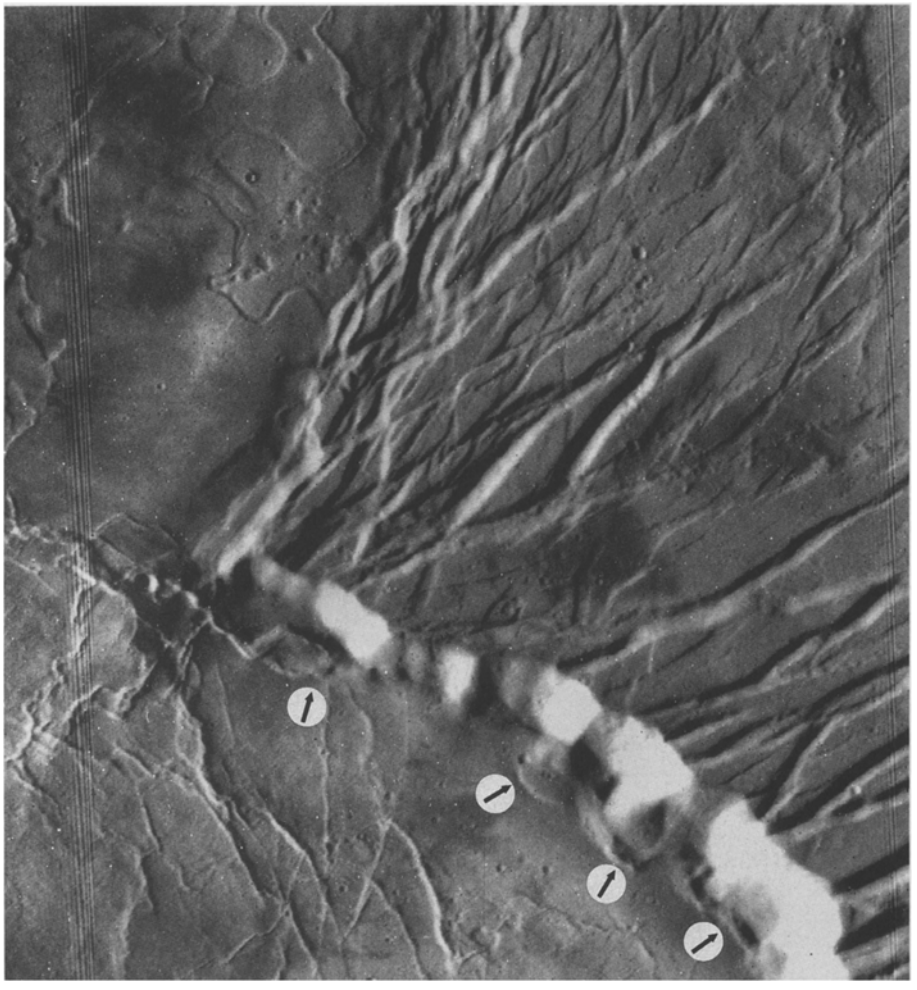

Fig. 11. View of the walls of craters 4 and 5 cutting the circumferential graben of crater 1. The illumination direction is from the left, and image width is equivalent to 14 km. The wall segment shown here is estimated from shadow-length measurements to be about 750 m high. Note the bench that surrounds the perimeter of the crater floor (*arrowed*) which we interpret to be a high-stand ledge produced by drainage of a lava lake. See Fig. 8b for location. Viking Orbiter frame 473S26 (14 m/pixel)

Stage 2: Crater 2 cuts the rim of crater 1, and so postdates the main collapse event, but stratigraphic relationships do not permit any more accurate determination of the time of formation of crater 2 to be determined, except that wrinkle ridges similar to those associated with Stage 7 are found on the floor of crater 2.

Continued subsidence of the central portion of crater 1 created an extensional environment close to the caldera wall and a compressional environment closer to the caldera center. Concentric graben and ridges formed at this time on the floor of crater 1 (Fig. 2). In conjunction with the subsidence associated with Stage 7 (see below), an additional 1300 ± 120 m of sagging occurred within crater 1 beyond the change in topography associated with the initial collapse.

Stage 3: New collapse events occurred at the western end of the caldera, forming the 1700 m-deep crater 3. After the solidification of the floor of crater 3, an episode of circumferential graben formation took place close to the wall of this part of the caldera, presumably due to the subsidence of the central portion of the floor.

Stage 4: Additional new subsidence events, located just south of the caldera center, formed craters 4 and 5. These events postdate the formation of the main caldera (crater 1) and crater 3 because the circumferential graben in crater 1 are cut by crater 4 (Fig. 11), and created scarps between the boundaries of craters 1, 3 and 5 at the northwestern edge of crater 5 (Fig. 2a).

Stage 5: On the basis of morphologic evidence for resurfacing (burial of earlier tectonic features and the creation of a smooth transition between the two segments of the caldera floor), the combined floor of craters 4 and 5 was probably occupied by a large lava lake during (or just after) its formation. The linear ridges are interpreted to be compressional features produced by local convergence and/or rafting of solidified lava plates on the surface of the lake surface. These ridges (Fig. 10) cross the boundaries of craters 4 and 5, indicating that both craters were flooded at the same time.

Stage 6: Partial drainage of the lava lake within crater 4 and 5 produced a bench around the perimeter of crater 4 (Figs. 9 and 11). High-resolution image data are not available to determine whether the perimeter of crater 5 also possesses such a bench.

Stage 7: Continued subsidence of the central portion of the summit area produced a compressional stress regime (Zuber and Mouginis-Mark 1990) that promoted the

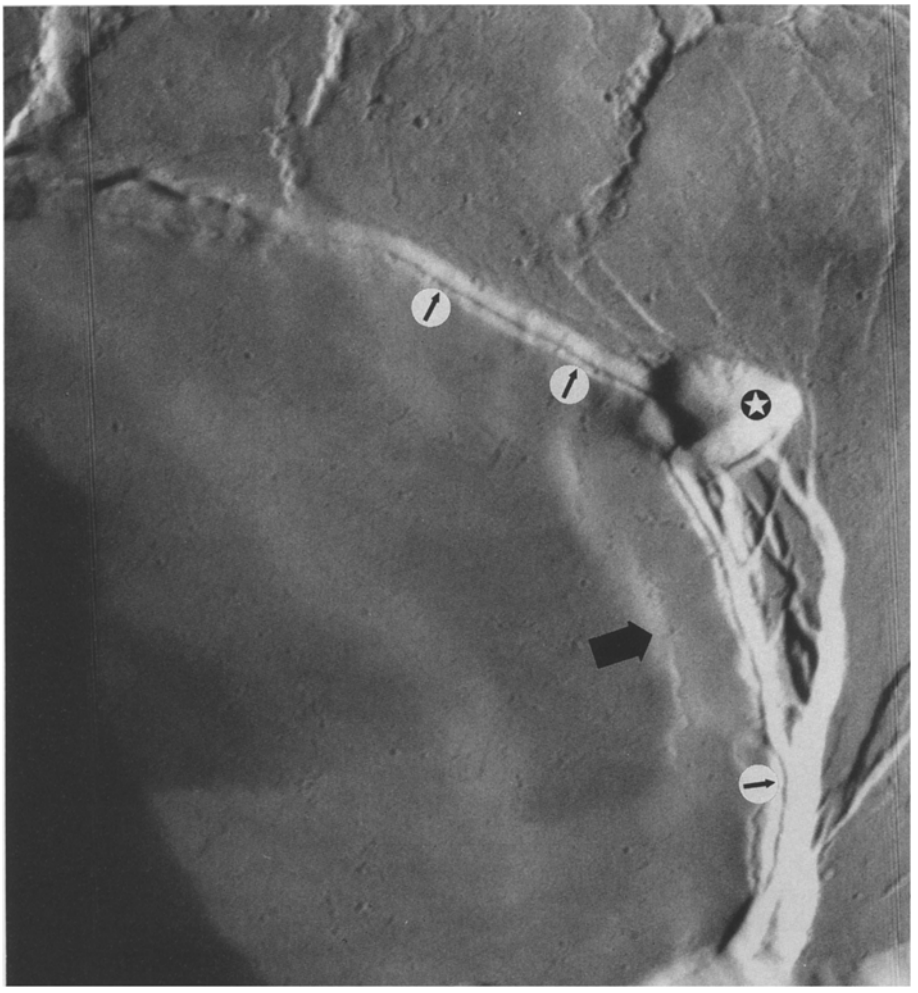

Fig. 12. Eastern portion of crater 6. Note the lack of evidence for tectonic deformation. A bench (*large arrow*) exists on the northeastern part of the crater floor, and a prominent horizon (*small arrows*) can also be seen in the wall rocks. The elongate depression of the rim of crater 6 (*) has been interpreted to be a monogenetic volcanic crater (Mouginis-Mark 1981). Illumination direction is from the left. See Fig. 8b for location. Viking Orbiter frame 474S23 (15 m/pixel)

formation of the large (>3 km wide) wrinkle ridges in craters 1, 2 and 5 (Fig. 6a). The numerous linear ridges formed in Stage 6 were thus preserved on top of these larger wrinkle ridges. These ridges are also seen on the floor of crater 2, so that it is likely that crater 2 had formed by this time (assuming the same tectonic event produced both sets of ridges).

Stage 8: The final collapse event, amounting to a displacement of ~350 m, produced crater 6. Unlike the events preserved on the floor of craters 4 and 5 (Stage 5), there is no evidence of surface features (i.e. linear ridges) that could be associated with overturning of the lake on the floor of crater 6. No wrinkle ridges indicative of large-scale subsidence or deformation can be seen within crater 6, but there is a prominent bench ~200 m above the main part of the crater floor. A second prominent discontinuity is also visible (Fig. 12) ~100 m above this bench, suggesting that multiple levels of a lava lake may have existed due to episodic draining of the erupted lava.

Discussion

Mouginis-Mark (1981) recognized that the floor of Olympus Mons shows little evidence for small-volume intra-caldera activity. No individual lava flows can be seen on any portion of the caldera floor, and there is only one 2.0×2.5 km crater that might be a monogenetic vent (Fig. 12). Inspection of the rim of the caldera (Fig. 13) shows that none of the flows on the uppermost flanks flowed into the caldera, and that all of the flows have been beheaded by subsequent collapse of the caldera rim. No evidence for incipient rift zones can be found.

There are several alternative ways to explain the observed ~2 km variation in rim topography of Olympus Mons, where the segments of the caldera surrounding the youngest nested craters were built to higher elevations than the rim segments around older collapse events (Fig. 5b). The mechanism that we favor is that the original caldera formed off-center from the top of the original cone (as has occurred at Mauna Loa, Hawaii). Alternatively, one side of the summit region may have subsided relative to the other, with the subsequent burial of the bounding faults by younger lava flows (as at Kilauea volcano, Hawaii; Holcomb 1987). A third option is that intrusive events associated with continued activity of Olympus Mons raised the rim crest at places where activity continued the longest. In this third case, we would expect to see extensional graben around this portion of the caldera rim, but no such features can seen. By analo-

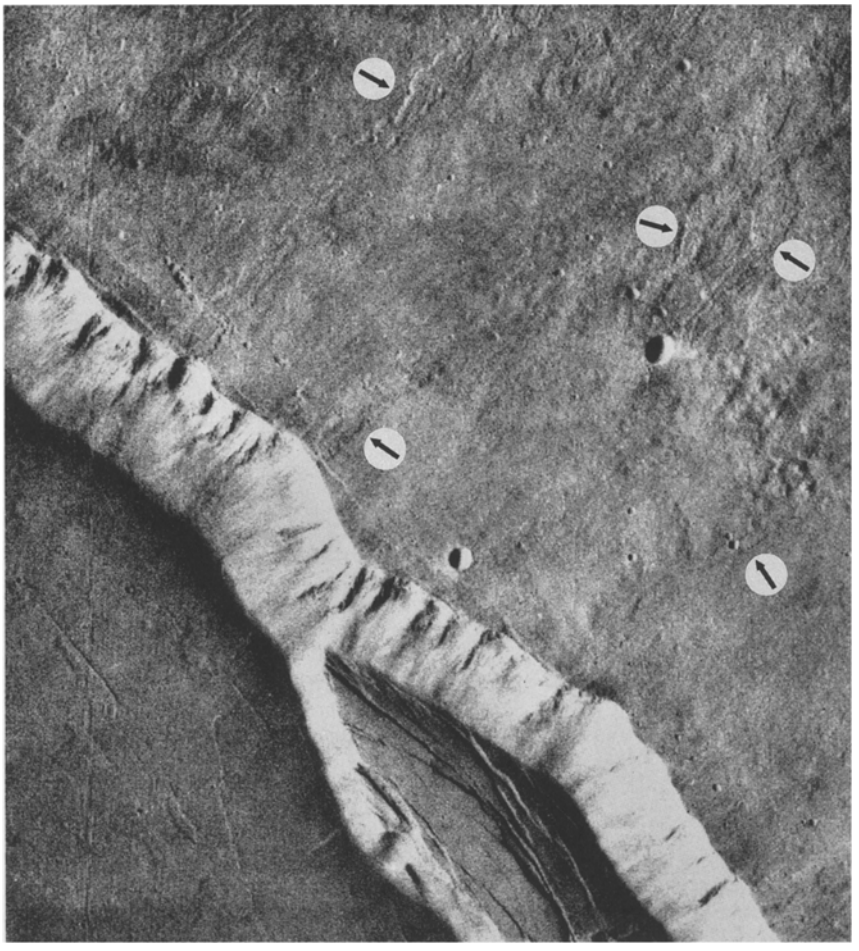

Fig. 13. Rim of crater 3 displaying lava flows (*arrowed*) that have been beheaded by caldera collapse events. Note that these flows traveled perpendicular to the present day rim. Illumination direction is from the left. See Fig. 8b for location. Viking Orbiter frame 360A32 (17 m/pixel)

gy with terrestrial shield volcanoes such as the Koolau volcano in Hawaii (Walker 1987), dike intrusions within Olympus Mons may not only cause horizontal displacements of the flanks of a volcano, but could also result in the vertical uplift (or down-sagging) of the summit area. Based upon the available Viking Orbiter images, however, we favor the simplest explanation for the variation in rim topography; i.e. that the Olympus Mons caldera originally formed off-center from the summit.

The sequence of collapse events and partial caldera infilling identified here demonstrates that Olympus Mons underwent a period of summit activity that in many respects was similar to that described for Hawaiian volcanoes (Walker 1987, 1988). These collapse events at Olympus Mons may have spanned thousands to a few millions of years, but there are insufficient data to constrain the exact duration of this activity. While all segments of the caldera floor possess craters that are interpreted to be of impact origin, we have not observed any pronounced difference in impact crater size/frequency curves for different segments of the caldera floor. Although the size of the caldera limits the statistical validity of crater counts, our observations imply that all of the volcanic events described in this study occurred in a relatively short time period compared to the entire geologic history of Mars (thought to exceed 4 billion years; cf. Scott and Carr 1978).

Our analysis also raises the question of why Olympus Mons is unique among Martian volcanoes in having well-preserved examples of large-scale subsidence of the caldera floor after sufficient time had elapsed to allow a solidified surface to form on the intra-caldera lava lake(s). Other Martian shields of comparable size to Olympus Mons show evidence of either extensional or compressional tectonism, but for no other volcano do well-formed examples of both sets of features exist. Within the caldera of Ascraeus Mons, the early collapse craters all have graben close to the caldera walls (Mouginis-Mark 1981), and Pavonis Mons has numerous wrinkle ridges across the central portion of the caldera floor (Crumpler and Aubele 1978). At Arsia Mons, block-faulting of the caldera rim has taken place but no compressional or extensional features can be found (Mouginis-Mark 1981), so that the second stage of summit subsidence seen at Olympus Mons either did not occur at Arsia Mons, or these tectonic features were subsequently covered by younger lava flows. Only at the much smaller (~170 km diameter) Apollinaris Patera do we find good morphological evidence for a two-state subsidence history for another Martian volcano, but neither graben nor wrinkle ridges can be found within the caldera of Apollinaris Patera.

Whereas the summit of Olympus Mons displays considerable migration in location (with respect to the cal-

dera rim) of the main caldera collapse events, the dimensions of the caldera are typical for Martian volcanoes. Arisa Mons has a caldera of greater width (~120 km); the largest segment of the caldera of Ascraeus Mons is ~40×38 km in diameter and ~3.1 km deep (Mouginis-Mark 1981); the caldera of Tharsis Tholus has a greater depth (>4 km; M Robinson, unpublished data 1990); and Alba Patera has two discrete calderas separated by more than 50 km (Carr 1981). Wood (1984) has hypothesized that the dimensions of planetary calderas reflect the size of the magma chamber, from which we infer that the internal structure (i.e. the size and location of a magma chamber) and the volume of erupted material from Olympus Mons were, to a first order, comparable to other Martian volcanoes. The absence of tectonic features on the floors of these other calderas may thus be due to the absence of slopes of the same scale as those that are found within the Olympus Mons caldera, or to subsequent activity that has covered the floor to a depth that is sufficient to bury wrinkle ridges and/or graben. The Mars Observer Laser Altimeter (MOLA), which will fly on the Mars Observer spacecraft to be launched in 1992, should provide many of the topographic data required for resolving these questions. Specific observations that MOLA could make would include slope measurements of the caldera floor, absolute height differences between adjacent segments of the caldera floor, and estimates of the total volume of subsidence association with each collapse. Differences between Olympus Mons and the other Martian volcanoes may not only help to understand the evolution of Olympus Mons, but may also provide insight into the collapse mechanism of terrestrial examples, such as Hawaiian calderas (e.g. Walker 1988) and Volcan Fernandina in the Galapagos Islands (Simkin and Howard 1970).

Summary and implications for terrestrial calderas

1. An eight-stage evolutionary sequence for the summit caldera of Olympus Mons volcano on Mars has been identified. This sequence included collapse events that produced 65 km diameter craters, lava lakes that may have been more than 30 km in width, and the protracted subsidence of the crater floor after the initial cooling of the lava lake surface.
2. Use of shadow-length measurements and photoclinometric profiles derived from Viking Orbiter images has revealed that as much as 2.5 km of collapse took place within the 80×65 km diameter caldera, and that the elevation of the caldera rim varies by almost 2.0 km. The formation of the caldera off-center from the summit of the volcano is favored to explain this variation in rim topography.
3. The caldera of Olympus Mons is unique for Martian volcanoes, in that geomorphic evidence for both extensional and compressional tectonism is prominently displayed. These tectonic features have been interpreted to be due to the deformation of a shallow magma chamber (Zuber and Mouginis-Mark 1990), raising the interesting implication that the magma chambers within other Martian volcanoes may have been at a greater depth within the volcanic edifices.
4. The Viking Orbiter data set for Olympus Mons provides a clear chronology of caldera collapse that on terrestrial volcanoes is often masked or destroyed by subsequent erosion and eruptions. Our observations may thus have significance for the interpretation of terrestrial calderas because continued subsidence within Olympus Mons can be demonstrated over a long (tens to hundreds of years?) period of time after the initial collapse. The duration of individual caldera collapse events may thus be longer than has been inferred from field observations (e.g. Simkin and Howard 1970), and may in fact be masked on the Earth by the higher frequency of eruptions.

In the case of Olympus Mons, it is also possible to infer that the spatial location of the magma chamber migrated within the edifice between successive collapse events. This magma chamber migration has been postulated for the Koolau Volcano of Hawaii (Knight and Walker 1988), but can only be inferred from the orientation of dikes preserved in the eroded volcano. Olympus Mons therefore provides a good demonstration of the value of studying planetary volcanoes in order to further understand basic volcanological processes that also occur on Earth.

Acknowledgements. This work has benefited from numerous discussions about Martian caldera tectonics with Maria T Zuber, NASA/Goddard Space Flight Center. Comments from Scott Rowland during the preparation of this manuscript are acknowledged. This manuscript was also improved by helpful reviews from Larry Crumpler and Chuck Wood. Special thanks are extended to Eric Eliason at the Astrogeology Branch, US Geological Survey, Flagstaff for recovering the digital data for Viking Orbiter Rev. 890A, under funding from the NASA Planetary Data System Project (Contract No. WO-8786). This research was supported by Grant NAGW-437 from NASA's Planetary Geology Program. This is Planetary Geosciences Publication #677, and SOEST Contribution #2810.

References

Carr MH (1981) The surface of Mars. Yale University Press, New Haven, Connecticut, 232 pp
Carr MH, Greeley R (1980) Volcanic features of Hawaii: a basis for comparison with Mars. NASA SP-403, 211 pp
Crumpler LS, Aubele JC (1978) Structural evolution of Arsia Mons, Pavonis Mons and Ascraeus Mons: Tharsis region of Mars. Icarus 34:496–511
Davis PD, Soderblom LA (1984) Modeling crater topography and albedo from monoscopic Viking Orbiter images 1. Methodology. J Geophys Res 89:9449–9457
Greeley R, Spudis PD (1981) Volcanism on Mars. Rev Geophys Space Phys 19:13–41
Holcomb RT (1987) Eruptive history and long-term behavior of Kilauea Volcano. Volcanism in Hawaii, US Geol Surv Prof Pap 1350:261–350
Knight MD, Walker GPL (1988) Magma flow directions in dikes of the Koolau Complex, Oahu, determined from magnetic fabric studies. J Geophys Res 93:4301–4319
Mouginis-Mark PJ (1981) Late-stage summit activity of Martian shield volcanoes. Proc Lunar Planet Sci 12B:1431–1447
Mouginis-Mark PJ, Robinson MS, Zuber MT (1990) Evolution of the Olympus Mons Caldera, Mars (abstract). Lunar Planet Sci XXI:815–816

Mouginis-Mark PJ, Wilson L, Zuber MT (1991) The physical volcanology of Mars. In: Mars, University of Arizona Press, Tucson, AZ, in press

Peck DL, Kinoshita WT (1976) The eruption of August 1963 and the formation of Alae Lava Lake, Hawaii. US Geol Surv Prof Pap 935-A

Plescia JB, Golombek MP (1986) Origin of planetary wrinkle ridges based on the study of terrestrial analogs. Geol Soc Am Bull 97:1289–1299

Robinson MS (1990) Precise topographic measurements of Apollinaris and Tyrrhena Patera, Mars (abstract). Lunar Planet Sci XXI:1027–1028

Scott DH, Carr MH (1978) Geologic Map of Mars. US Geol Surv Misc Map I-1083

Sharpton VL, Head JW (1988) Lunar mare ridges: analysis of ridge-crater intersections and implications for the tectonic origin of mare ridges. Proc Lunar Planet Sci Conf 18:307–317

Simkin T, Howard KA (1970) Caldera collapse in the Galapagos Islands, 1968. Science 169:429–437

Walker GPL (1987) The dike complex of Koolau volcano, Oahu: internal structure of a Hawaiian rift zone. US Geol Surv Prof Pap 1350:961–993

Walker GPL (1988) Three Hawaiian calderas: an origin through loading by shallow intrusions? J Geophys Res 93:14773–14784

Wood CA (1984) Calderas: a planetary perspective. J Geophys Res 89:8391–8406

Wu SSC, Garcia PA, Jordan R, Schafer FJ, Skiff BA (1984) Topography of the shield volcano, Olympus Mons on Mars. Nature 309:432–435

Zuber MT, Mouginis-Mark PJ (1990) Constraints on the depth and geometry of the magma chamber of the Olympus Mons volcano, Mars (abstract). Lunar Planet Sci XXI:1387–1388

Editorial responsibility: S Carey